Foreshock compressional boundary

N. Omidi,[1] D. G. Sibeck,[2] and X. Blanco-Cano[3]

Received 26 November 2008; revised 1 April 2009; accepted 26 May 2009; published 12 August 2009.

[1] We employ 2.5-D electromagnetic, hybrid simulations that treat ions kinetically via particle-in-cell methods and electrons as a massless fluid to study the formation and properties of a newly discovered boundary named the foreshock compressional boundary (FCB). This boundary forms in the ion foreshock and is associated with enhanced densities and magnetic field strengths. At times, but not always, the FCB separates the pristine solar wind plasma from the ion foreshock. In this study, we investigate the dependence of FCB characteristics on solar wind Mach number and cone angle (the angle between flow velocity and interplanetary magnetic field). We show that the strength of the foreshock compressional boundary increases with the Mach number. This enhancement is in turn tied to the density and velocity of the backstreaming ions in the foreshock whose interaction with the solar wind results in ULF turbulence which is ultimately responsible for the formation of FCB. During small cone angles the foreshock compressional boundary is symmetric with respect to the radial direction. As the cone angle increases, the FCB becomes less symmetric and eventually is confined to one side of the foreshock. The strength of the FCB also decreases with increasing cone angle but depending on the Mach number can exist for cone angles of 40° and beyond. A recent study that compared data from a global hybrid simulation of the foreshock with Cluster spacecraft observations showed that encounters with foreshock cavities can be interpreted as back and forth motion of a FCB causing spacecraft to move from the solar wind through the FCB into the foreshock and back into solar wind. An example of a FCB observed by the Cluster spacecraft is presented and shown to be in general agreement with model predictions.

Citation: Omidi, N., D. G. Sibeck, and X. Blanco-Cano (2009), Foreshock compressional boundary, *J. Geophys. Res.*, *114*, A08205, doi:10.1029/2008JA013950.

1. Introduction

[2] Early spacecraft observations revealed that the bow shock is associated with ion reflection and leakage toward the upstream, resulting in a region called the ion foreshock [*Asbridge et al.*, 1968; *Greenstadt et al.*, 1968]. These backstreaming ions originate from the quasi-parallel portion of the bow shock, where the shock normal makes an angle of ~45° or less with the upstream magnetic field. Later observations established that the backstreaming ions form a variety of velocity distribution functions that range from field aligned beams to highly scattered and heated distribution functions called diffuse ions (see *Fuselier* [1995] for a detailed review). Also, a variety of ULF waves have been observed in association with the backstreaming ions (e.g., *Hoppe et al.* [1981] and review by *Russell and Hoppe* [1983]).

[3] Historically, two boundaries have been identified in association with the ion foreshock. One is the boundary separating the pristine solar wind from field aligned, backstreaming ion beams on magnetic field lines connected to the bow shock [*Asbridge et al.*, 1968; *Gosling et al.*, 1978; *Paschmann et al.*, 1979; *Bonifazi et al.*, 1980a, 1980b]. This boundary is typically referred to as the ion (beam) foreshock boundary. The interaction of the field aligned ion beams with the solar wind results in the generation of parallel propagating (~30 s period) sinusoidal waves [*Gary et al.*, 1981]. Although propagating sunward, these waves are carried back by the solar wind as they grow in amplitude. As a result, ULF wave activity is not detected at the ion foreshock boundary but at another boundary further downstream, identified as the ULF foreshock boundary [*Greenstadt et al.*, 1980].

[4] In addition to ion beams and ULF waves, another phenomenon associated with the foreshock and discovered by *Sibeck et al.* [2002] is an isolated event observed in time series data known as foreshock cavities. The events are associated with changes in solar wind parameters such as density, velocity, temperature and magnetic field. The core of the event is associated with decreases in both density and total magnetic field and is surrounded by regions of increased density and magnetic field. The core is also associated with increase in ion temperature and drop in flow velocity. Foreshock cavities were originally thought to be spatial structures created through solar wind interaction with

[1]Solana Scientific Inc., Solana Beach, California, USA.
[2]NASA Goddard Space Flight Center, Greenbelt, Maryland, USA.
[3]Ciencias Espaciales, Instituto de Geofisica, Universidad Nacional Autonoma de Mexico, Coyoacan, Mexico.

Copyright 2009 by the American Geophysical Union.
0148-0227/09/2008JA013950

the backstreaming ions. However, recently a new interpretation has been offered by *Sibeck et al.* [2008] that is more consistent with both observations and simulations.

[5] *Sibeck et al.* [2008] presented results from a 2.5-D global hybrid (kinetic ions, fluid electrons) simulation of the dayside magnetosphere during radial interplanetary magnetic field (IMF) direction. They noted the presence of a boundary on one side of the foreshock that was associated with enhanced densities, magnetic field strengths and temperatures. The level of these enhancements diminishes with distance from the bow shock. The plasma and field conditions on one side of this boundary correspond to the pristine solar wind and on the other side to the ion foreshock. The IMF field lines threading through the boundary do not represent either the first or the last lines connected to the bow shock. Although, originally referred to as the foreshock boundary, the name foreshock compressional boundary (FCB) is more descriptive and adopted here. On the basis of the properties of the foreshock compressional boundary, *Sibeck et al.* [2008] proposed that the back and forth motion of the FCB across a spacecraft would result in field and plasma signatures similar to those associated with foreshock cavities. This interpretation was further supported through a detailed comparison between the simulation results and Cluster observations.

[6] The compressional foreshock boundary shown by *Sibeck et al.* [2008] represents the first time this boundary has been seen in a global hybrid simulation, suggesting that it does not form under all solar wind conditions. The relatively frequent observations of foreshock cavities, on the other hand suggest that FCBs are a common feature of the ion foreshock structure. The purpose of this study is to understand under what solar wind conditions FCBs form and the extent to which solar wind modifies their properties. To this end, we first examine the Mach number dependence of FCB formation during radial IMF conditions and show that their strength is enhanced with increasing flow speed. This enhancement is associated with the increase in density and velocity of the backstreaming ions. Next, we show that the foreshock compressional boundary forms during radial and quasi-parallel IMF cone angles (i.e., flow and IMF angles $\sim$40°). During small cone angles the FCB is symmetric with respect to the Sun-Earth line direction, however, this symmetry breaks down as the cone angle increases until eventually the FCB only forms on one side of the foreshock. In this study, we employ both global and local hybrid simulations which are described in section 2. Section 3 describes the simulation results and also shows an example of a FCB observed by the Cluster spacecraft, while section 4 gives a summary and conclusions.

2. Hybrid Simulation Model

[7] The main tools of investigation are 2.5-D (2-D in space and 3-D in currents and electromagnetic fields) global and local hybrid simulations used extensively in the past [e.g., *Omidi et al.*, 2004, 2005; *Omidi and Sibeck*, 2007]. In electromagnetic hybrid codes, ions are treated as macroparticles and consist of one or more species (e.g., differing mass, charge, etc.) whereas electrons are treated as a massless, charge neutralizing fluid [see, e.g., *Winske and Omidi*, 1993, 1996]. The details of the global hybrid model are described by *Omidi et al.* [2005] and a brief description is given here.

[8] The simulation plane lies in the X-Y plane with X along the solar wind flow direction (Sun-Earth line). The simulation box extends 1500 ion skin depths (c/ω_p, where c is the speed of light and ω_p is the ion plasma frequency) in the X direction and 1200 in the Y direction with cell size of 1 ion skin depth. The number of particles per cell in the solar wind is 15. To improve the statistics of the backstreaming ions, each particle is split into 16 smaller particles with the same charge to mass ratio [*Lapenta*, 2002]. The solar wind electron and ion betas (ratio of kinetic to magnetic pressure) are each set to 0.5.

[9] The IMF lies in the X-Y plane, and makes an angle of θ (cone angle) with the x axis. In this study, θs in the range of 0° to 40° are considered. The solar wind is continuously injected along the X direction, from the left boundary and allowed to leave the system from the remaining three boundaries. Solar wind flow speeds corresponding to Alfven Mach numbers ranging from 6 to 15 are considered in the study. To form the bow shock and foreshock we use a circular reflecting boundary as the obstacle to solar wind flow. In the simulation run shown by *Sibeck et al.* [2008], a magnetic dipole with a tilt angle of 20° was used as the obstacle. Despite the radial IMF direction, the presence of the dipole tilt breaks the symmetry of the magnetopause and bow shock about the Sun-Earth line and as a result, FCB forms on only one side of the foreshock. The use of a circular, plasma reflecting obstacle removes this possibility and allows us to investigate the symmetry properties of the foreshock compressional boundary as a function solely of the upstream solar wind conditions. The obstacle is centered at X = 1100, Y = 600 and has a diameter of 200 c/ω_p.

[10] We should note that while the size of the simulated bow shock is comparable to that of Mercury (i.e., smaller than Earth's) the results presented here are applicable over a wide range of scales. This is because the simulated bow shock and ion foreshock are not sensitive to the size of the system as long as this size is much larger than ion kinetic scales [see, e.g., *Omidi et al.*, 2004, 2005; *Blanco-Cano et al.*, 2006; *Omidi and Sibeck*, 2007].

[11] In order to understand the role of ion beam density, velocity and temperature on the formation of the compressional foreshock boundary we also use local hybrid simulations as described here. The simulation lies in the X-Y plane with periodic boundary conditions in the X direction and nonperiodic boundary conditions in the Y direction. The size of the box corresponds to 500 c/ω_p in the X direction and 800 c/ω_p in the Y direction. The cell size is 1 ion skin depth with 15 particles per cell representing the solar wind protons. We also use 15 particles per cell for the backstreaming proton beam, but give their contributions to plasma density a smaller weight to correspond to the beam density chosen for the run. A solar wind type plasma (same beta as above) is present throughout the simulation box moving from left to right. The backstreaming ions are present for all X but are confined to $200 \leq Y \leq 600$. This allows for the formation of the foreshock compressional boundary at the interfaces between the pristine solar wind and the solar wind with backstreaming ion beams. This model is similar to that used by *Thomas and Brecht* [1988] to investigate the formation of diamagnetic cavities in the

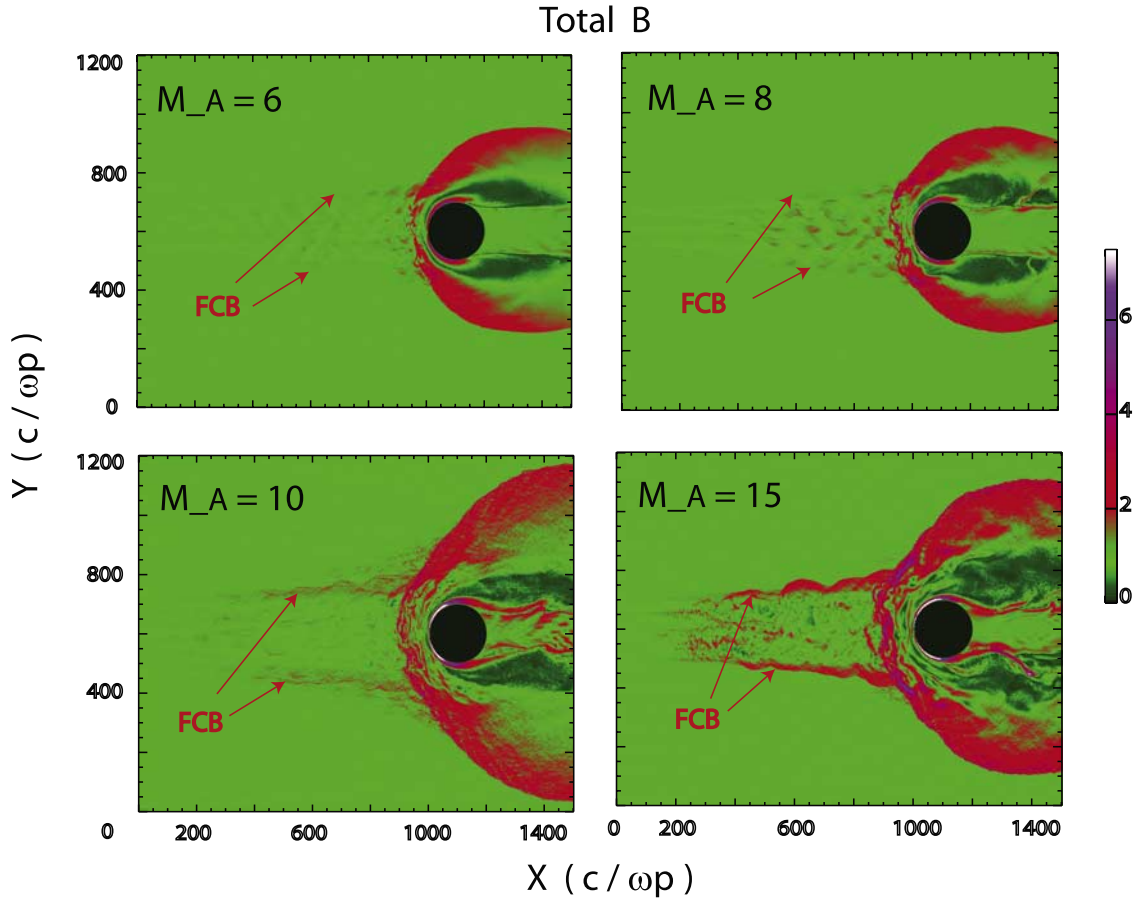

Figure 1. Color intensity plot of total magnetic field for four values of Mach number. Intensification of the foreshock compressional boundary with Mach number is evident.

solar wind. However, the size of the simulation domain in this study is much larger. The backstreaming ions have the same velocity as the solar wind but move from right to left (i.e., opposite of the solar wind). This study uses beam densities in the range of 1% to 2.5% of solar wind, velocities between 10 and 30 times the Alfven speed in the solar wind, and temperatures from 2 to 20 times that of solar wind protons. The background magnetic field is along the x axis.

3. Description of the Results

3.1. Mach Number Dependence of the FCB

[12] To examine the Mach number dependencies of the foreshock compressional boundary we use global hybrid simulations with a radial IMF orientation. Figures 1 and 2 show the total magnetic field strength and plasma density from four runs, corresponding to solar wind flow speed of 6–15 times the Alfven speed (V_A). Both magnetic field and density are normalized to their upstream values and to make the comparison between the four cases easier we choose a fixed scale ranging from 0 to 7.5. Enhancements of density and magnetic field labeled FCB are evident in Figures 1 and 2. The enhancements in density and magnetic field are colocated and correlated indicating that the foreshock compressional boundary is in the fast magnetosonic mode.

[13] It is evident from Figures 1 and 2 that the jumps in density and magnetic field associated with the FCB increase with higher flow speeds, i.e., the FCB is enhanced by increasing Mach number. Inside the foreshock, oscillations in density and magnetic field are evident corresponding to compressions and rarefactions associated with the generation and nonlinear evolution of ULF waves. The nature of the waves generated during radial IMF geometry is described by *Omidi* [2007] and *Blanco-Cano et al.* [2009], who showed the presence of right or left hand polarized sinusoidal waves propagating along the magnetic field and fast, linearly polarized, oblique (FLO) waves. Interaction and nonlinear coupling between these two classes of waves result in regions of density and magnetic field depletion surrounded by regions of field and density enhancement. While the signature of these structures resembles those of foreshock cavities, a major distinction between them is that foreshock cavities are isolated events in the solar wind while the regions of density and field depletion associated with the ULF wave activity are embedded in turbulence. To distinguish between the two, density and field depletions associated with ULF waves are given the name foreshock cavitons. *Blanco-Cano et al.* [2009] presented foreshock cavitons observed by the Cluster spacecraft and showed that their properties are similar to those of the simulated cavitons.

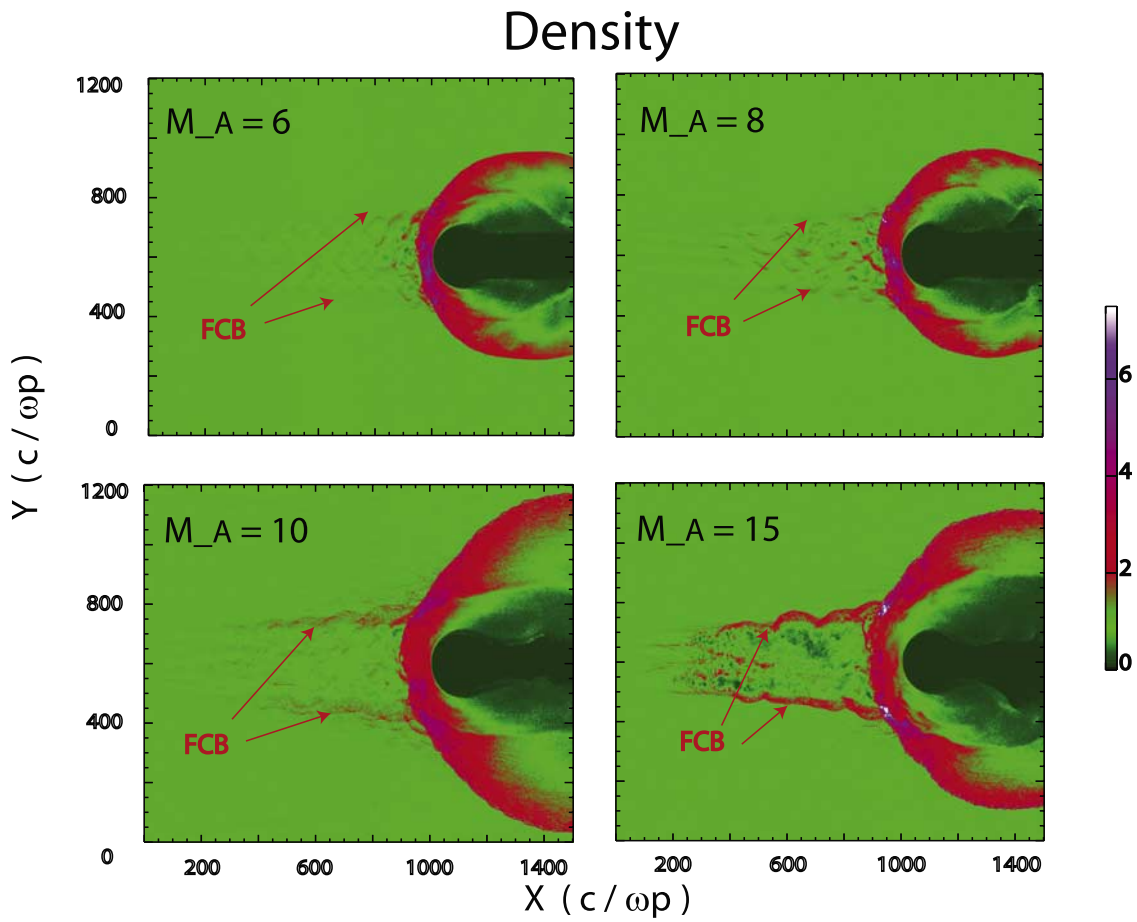

Figure 2. Plot of density for the same runs in Figure 1. The enhancements of density and magnetic field associated with FCBs are correlated, indicating a fast magnetosonic mode.

[14] Figures 1 and 2 show that as the Mach number increases, the density and field depletions associated with the cavitons become larger in amplitude and on a global scale, the foreshock is associated with bigger regions of field and density depletions and enhancements. To further demonstrate the changes in the FCB and foreshock properties as a function of Mach number, Figure 3 shows values of density, temperature, flow speed in X and Y directions and total magnetic field along trajectories starting on one side of the foreshock and ending on the other side. The trajectories are straight lines and their starting and end coordinates are shown in Figure 3. Note the change in scales from one Mach number to the other in Figure 3 which is necessitated by the fact that both the jumps in density and field associated with the FCB and the level of fluctuations in the foreshock increase with increasing Mach number.

[15] Figure 3 (top left), corresponding to Alfven Mach number of 6, shows that the density and field changes associated with the FCB are correlated and as high as ~40% of their background values. These are comparable to the levels of fluctuations within the foreshock region. Also, the two FCBs are not identical although on average the strength of the FCBs on both sides of the foreshock is comparable. The modest temperature increase outside of the FCBs in the solar wind is due to the presence of backstreaming ions. This demonstrates that in general the FCB and the ion foreshock boundary do not coincide. As such, the FCB does not represent the boundary between the quasi-parallel and quasi-perpendicular portions of the bow shock but rather separates a highly modified solar wind due to wave particle interactions from an unperturbed solar wind which may still include backstreaming ions (see further discussion of this point in sections 3.3 and 4). The presence of backstreaming ions upstream of the FCBs also result in decreases in flow speed along the X direction (Vx). On the other hand, the first major change in Vy is associated with the FCBs. This change in Vy, is in the opposite directions at the 2 FCBs and corresponds to flow away from the Sun-Earth line.

[16] Figure 3 (top right), corresponding to Alfven Mach number of 8, shows stronger and steeper FCBs. Also, the presence of the backstreaming ions upstream of the FCBs results in bigger changes in Vy, however, the biggest change still occurs at the FCBs. This trend continues with increasing flow speed so that while at lower Mach numbers the FCB corresponds to a fast magnetosonic wave pulse, at Mach numbers of ~>8 it exhibits shock-like behavior. The local normal to the boundary lies nearly perpendicular to the solar wind flow direction, but varies a bit because of surface corrugations. Given the fact that the FCB participates in the flow diversion around the obstacle, it can be viewed as an extension of the bow shock, particularly at higher Mach numbers where the jumps in density and magnetic field are comparable to those occurring at the bow shock.

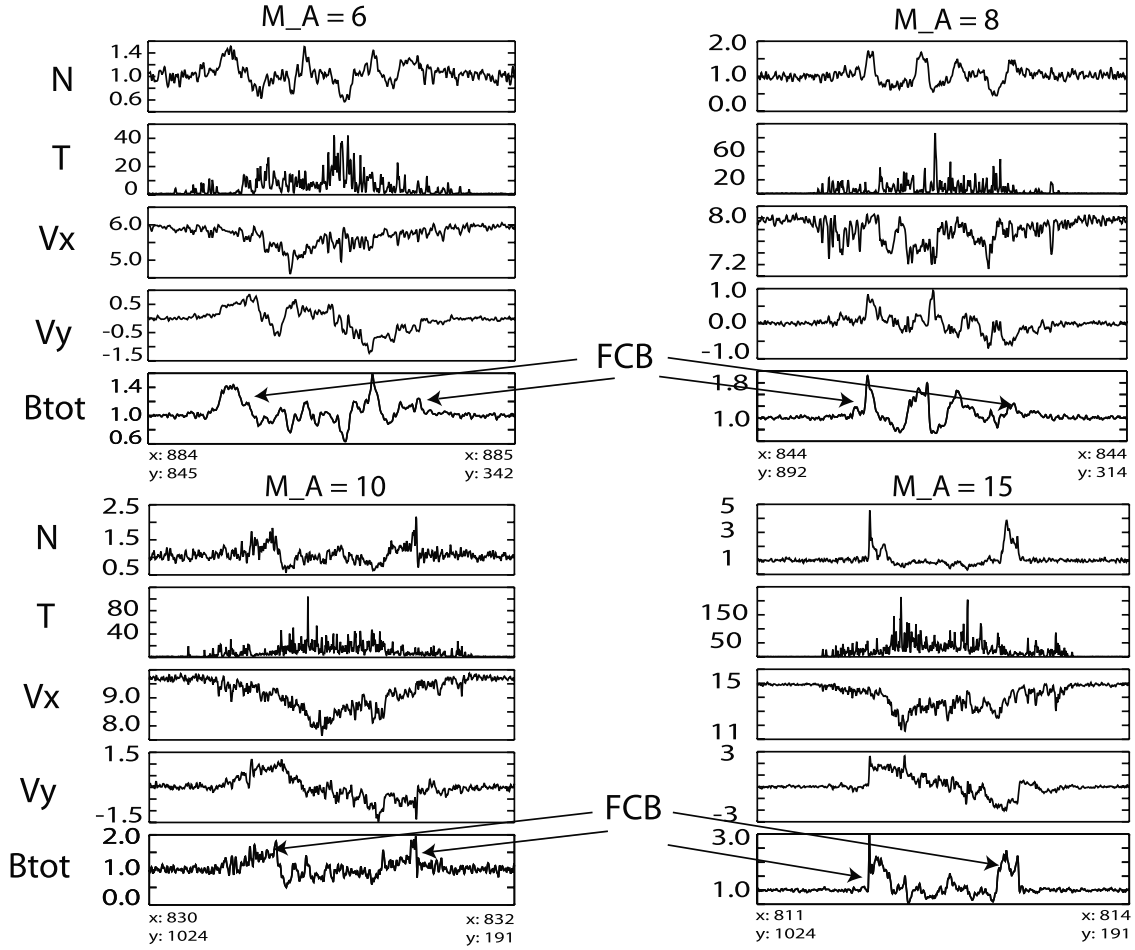

Figure 3. Cuts showing density, ion temperature, flow velocity in the X and Y directions, and total magnetic field for the four runs shown in Figure 1. The cuts are along straight line trajectories with the coordinates of starting and ending points indicated for each Mach number.

3.2. Impact of Ion Beam Properties on the FCB

[17] The Mach number dependence of the foreshock compressional boundary discussed above is ultimately tied to the properties of the backstreaming ion beams and their interaction with the solar wind. To examine the dependence of the FCB on the properties of the backstreaming ions we use the local hybrid model described in section 2. In this model the solar wind moves from left to right, while field-aligned ion beams move from right to left with equal speeds that mimic a specular reflection process at the shock. In particular, the effects of beam velocity, density and temperature on the FCB formation are considered. In regards to beam temperature, we find no major impact for the range of 2 to 20 times the solar wind temperature and therefore show only results from runs with the latter beam temperature.

[18] Figures 4, 5 and 6 show the density and magnetic field strength from 3 runs with beam densities 1% that of the solar wind, but beam speeds corresponding to relative velocities of 10, 20 and 30 V_A to solar wind. This corresponds to flow Mach numbers of 5, 10 and 15. For this range of beam speeds, a variety of resonant and nonresonant instabilities are possible with maximum growth rates along the magnetic field [e.g., *Gary et al.*, 1981]. We have conducted detailed linear theory for the beam properties considered here and find that in addition to the parallel propagating waves, fast magnetosonic waves with large wave normal angles are also unstable with growth rates comparable to the parallel propagating waves. These correspond to the FLO waves observed in the simulations. The details of the linear theory and the properties of the waves observed in the simulations will be presented in an accompanying paper in the near future. Here we concentrate on the foreshock compressional boundary.

[19] Considering Figure 4, the presence of density and magnetic field enhancements at the interface between the pristine solar wind and solar wind plus beam region is evident. As in the case of the foreshock compressional boundary, the density and magnetic field enhancements are correlated indicating a fast magnetosonic mode. The jumps in density and field are about 20% of the background and are consistent with our expectations for FCBs associated with a Mach 5 bow shock. Increasing the relative (to solar wind) beam speed to 20 V_A, leads to a much stronger FCB as shown in Figure 5. Specifically, density jumps of the order of 40–50% occur in association with the FCBs. Figure 6 shows that the density enhancements associated with the compressional boundary are even higher at 100% or more for beam speed of 30 V_A. Thus, it is evident that

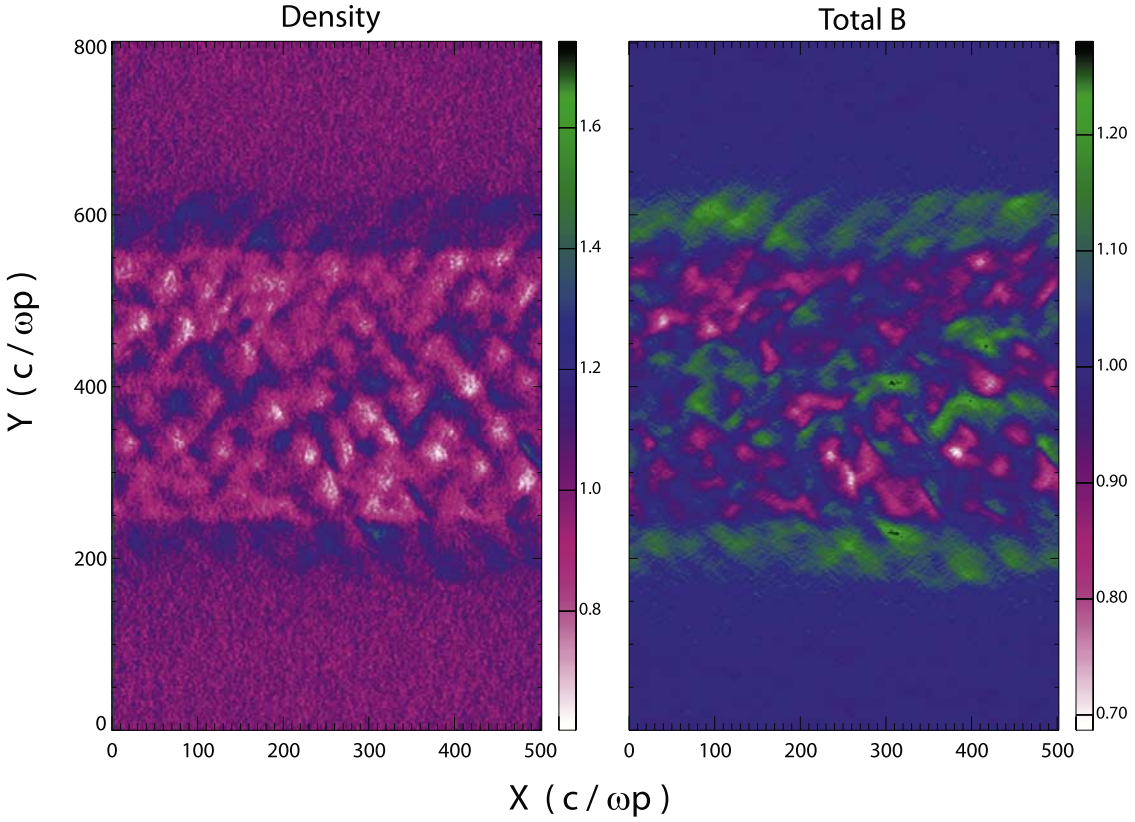

Figure 4. Plot of density and total magnetic field from a local hybrid run corresponding to beam density of 1% and velocity of 10 V_A.

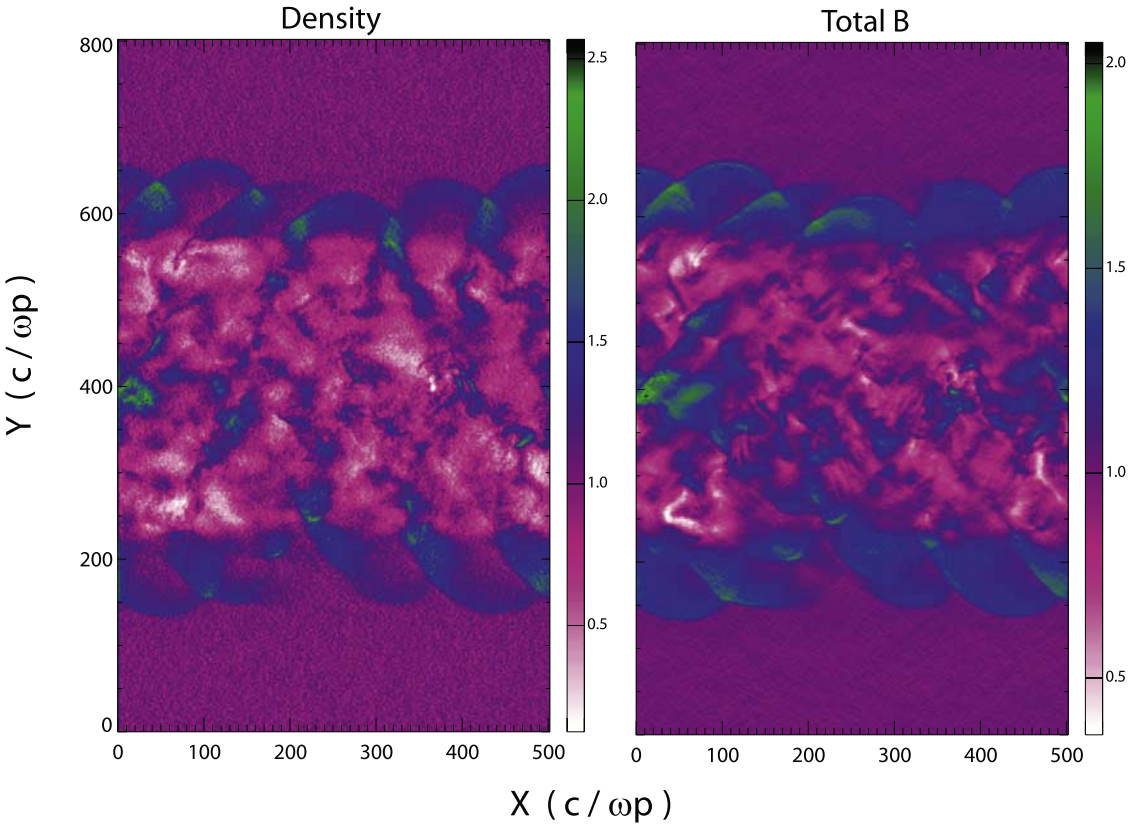

Figure 5. The same as Figure 4 except beam velocity is 20 V_A.

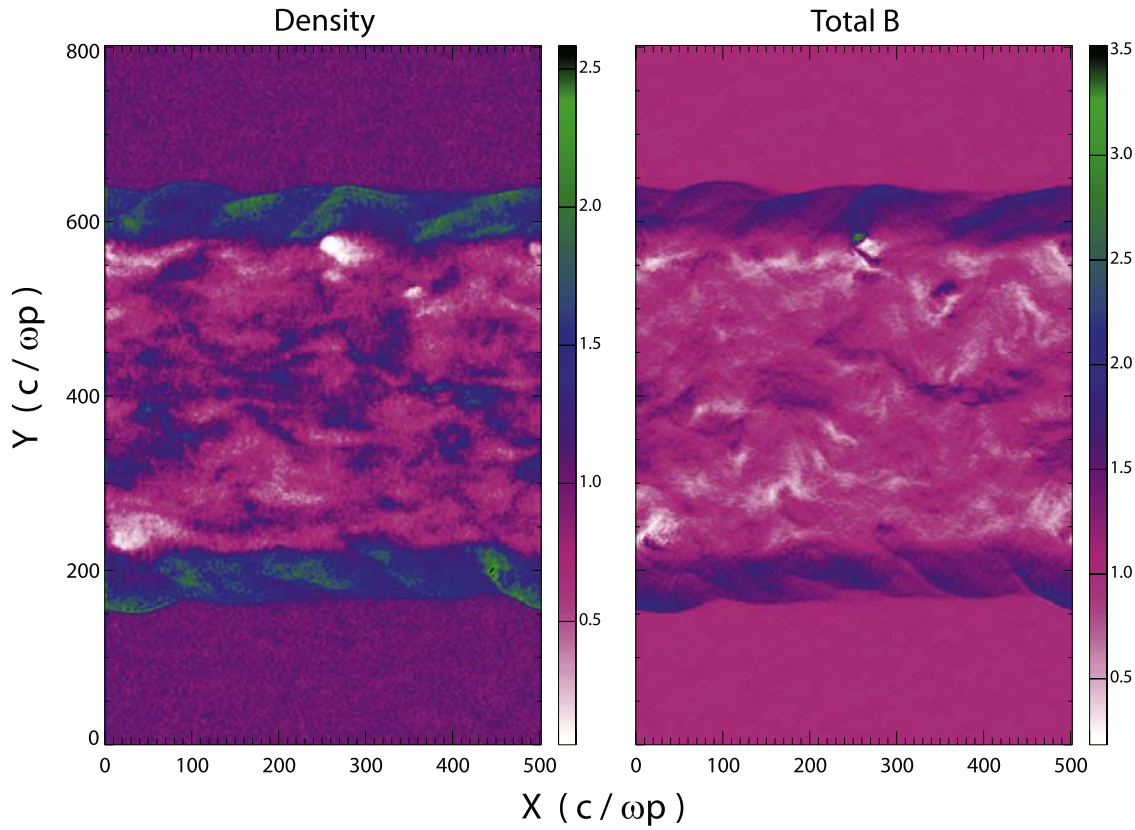

Figure 6. The same as Figure 4 except beam velocity is 30 V_A.

increasing the beam speed leads to a stronger foreshock compressional boundary.

[20] To examine the effects of beam density on the FCB properties, Figure 7 shows the density and magnetic field from a run corresponding to beam density of 2.5% and velocity of 10 V_A. This is in contrast to Figure 4 where the beam density is 1%. Comparing Figures 4 and 7 shows that increasing the beam density changes the density jump associated with FCB from 20% to 40% of the solar wind level. Thus, as in the case of beam velocity, increasing beam density results in strengthening of the foreshock compressional boundary. Comparing the changes associated with beam velocity and density suggests that the former effect is more pronounced.

3.3. Effects of Solar Wind Cone Angle on the FCB

[21] To illustrate the impact of the solar wind cone angle on FCB properties, Figures 8 and 9 show total magnetic field and density from three runs corresponding to cone angles of $\theta = 10°$, 20° and 40° and Alfven Mach number of 12. For $\theta = 10°$, a pair of FCBs form with the upper one clearly falling inside the ion beam and ULF foreshock boundaries by virtue of the fact that density and field perturbations can be found just outside of bow shock beyond the upper FCB. This example again illustrates that the FCB and ion beam and ULF foreshock boundaries generally do not coincide. This is because the regions of the foreshock connected to the parallel portion of the bow shock form faster while those connected to the quasi-parallel portions of the shock form slower. Thus, the foreshock region associated with the (nearly) parallel bow shock forms first resulting in FCBs, while ion beams and ULF waves associated with the quasi-parallel bow shock appear later and beyond where the FCB forms. This is the case for the upper FCB at $\theta = 10°$, but not the lower FCB, below which is mostly pristine solar wind.

[22] For $\theta = 20°$, Figure 8 shows that only one FCB forms in the lower portion of the ion foreshock region. This asymmetry is attributed to the variation of the ion beam properties along the parallel and quasi-parallel portions of the bow shock. As illustrated earlier, the formation and the strength of the FCB is tied to the density and velocity of the backstreaming ions and therefore, variations in beam properties originating from different parts of the bow shock can lead to asymmetric FCBs. This asymmetry results in either a pair of FCBs with different strengths, or complete elimination of one of the FCBs depending on the cone angle (and Mach number). Figure 9 shows the formation of a single FCB at cone angle of 40°, demonstrating that they can form over a broad range of cone angles. The maximum cone angle at which FCBs form depends on and increases with the Mach number. Examination of the FCB in Figure 9 shows that it falls inside the ion foreshock boundary and ion beams are found below the FCB.

3.4. Example of a FCB Observed by the Cluster Spacecraft

[23] Our simulation results show that foreshock compressional boundaries should form commonly upstream from the Earth's bow shock. Using Cluster magnetic field and plasma data we have been able to identify FCB crossings for a variety of solar wind speeds and IMF geometries, with

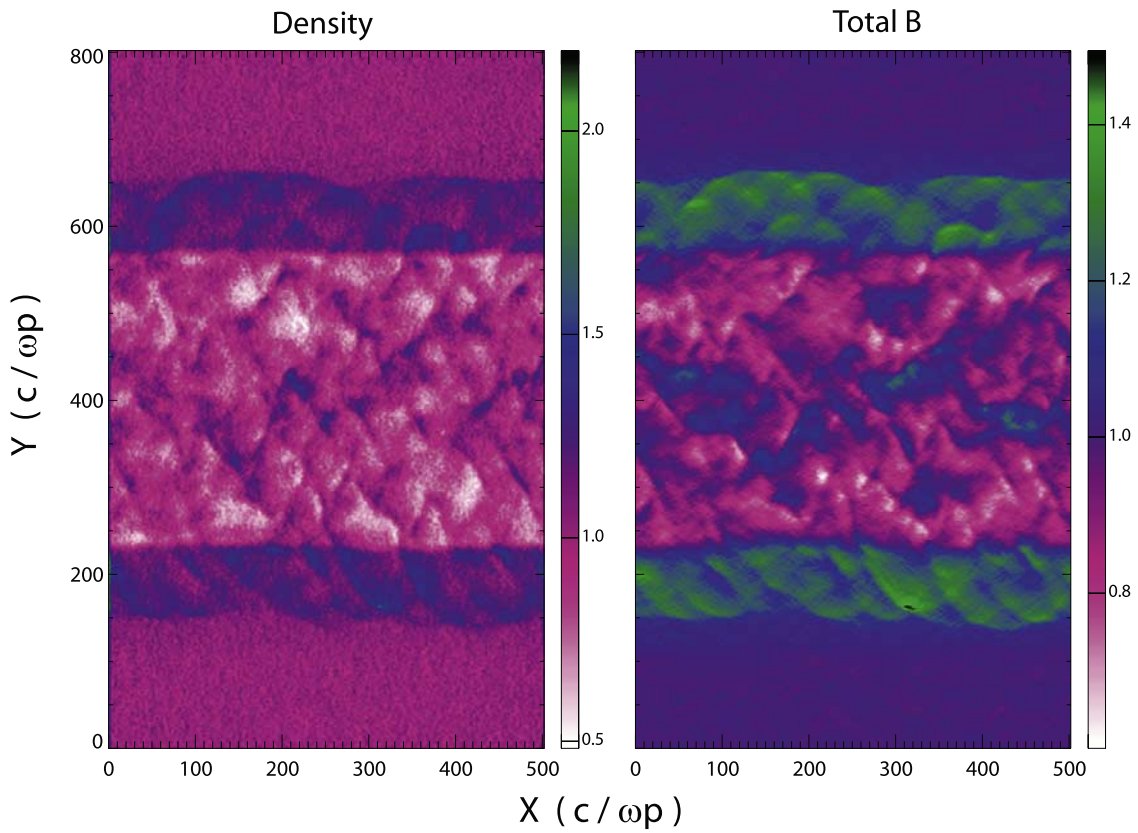

Figure 7. The same as Figure 4 except beam density is 2.5% of solar wind density.

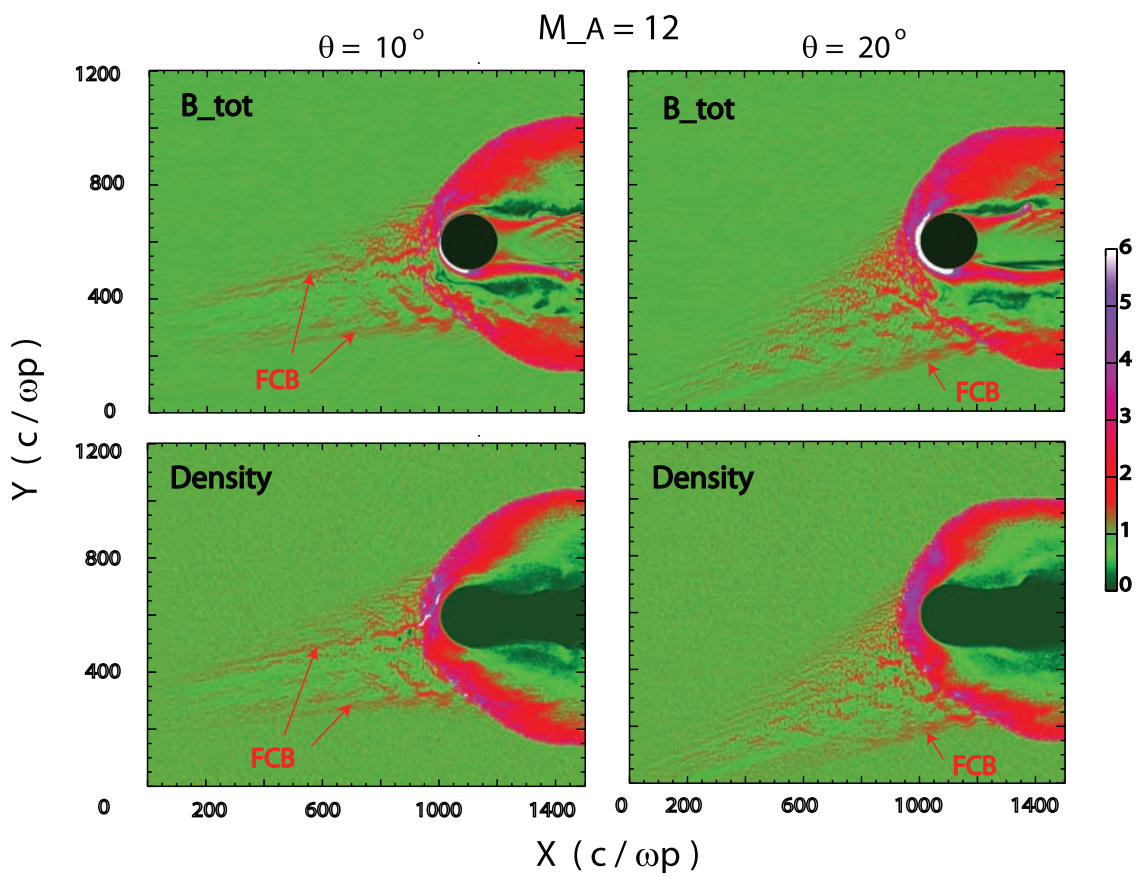

Figure 8. Plots of total magnetic field and density for runs corresponding to cone angles of 10° and 20°.

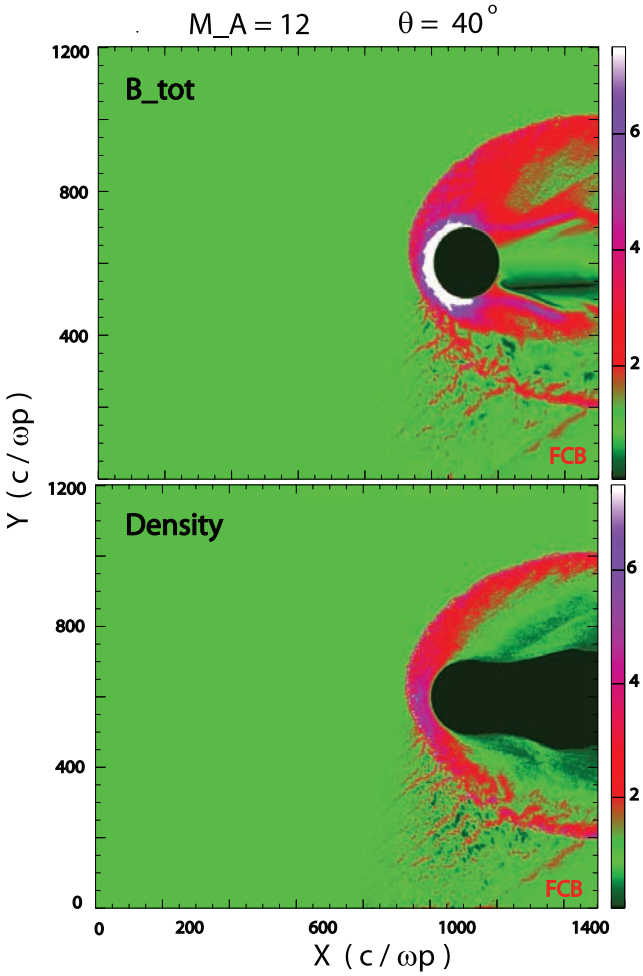

Figure 9. Plots of total magnetic field and density for a run corresponding to cone angle of 40°.

cone angles up to 50°. The properties of the observed FCBs and their dependence on solar wind conditions will be discussed in detail in a future manuscript. To illustrate the resemblance between the simulated FCBs and an observed boundary crossing, Figure 10 shows density, velocity components and magnetic field magnitude for an interval on 18 February 2002, when Cluster 1 position was GSE(x, y, z) = (9.88, 5.32, 8.09) R_E. During this interval the angle between the IMF and the flow was 42°, and the solar wind speed was ~7 V_A. The location of the observed FCB with respect to the bow shock is shown in Figure 10 (right) using asterisks in GSE X-Y and X-Z planes. The shape of a nominal bow shock was found using a parabolic shock as done by *Narita et al.* [2004] and the values that these authors obtained for the standoff distance and the flaring parameter for a similar interval on the same day of Cluster observations. The trajectory of Cluster 1 between 8:00–10:00 UT is shown as solid lines crossing the asterisks and moving in the direction of positive X. Also shown are the projections of the IMF vector onto the X-Y and X-Z planes.

[24] In Figure 10, we use magnetic field data with a resolution of 5 vectors per second [*Balogh et al.*, 2001] and spin resolution plasma moments from the CIS instrument [*Reme et al.*, 2001]. The FCB was crossed from the foreshock into the solar wind at 0905:00. In agreement with Figure 3, before the boundary is encountered, large amplitude compressive waves permeate the foreshock. We find that the characteristics of the observed boundary are consistent with our model predictions. The FCB is on the magnetosonic mode with B and N well correlated, and as shown in the Vy and Vz plots, the flow is deflected through the boundary. The high-frequency waves observed on the magnetic field magnitude after the FCB has been crossed indicate the existence of backstreaming particles, and the fact that this boundary does not always coincide with the ion and ULF foreshock boundaries.

4. Summary and Conclusions

[25] We presented results from global hybrid simulations that show the formation of a new boundary called the foreshock compressional boundary. This boundary is associated with correlated enhancements of density and magnetic field and is on the fast magnetosonic branch. During radial and small cone angles, a pair of relatively symmetric FCBs form on the opposite sides of the foreshock (in 2-D, whereas in 3-D we expect a semicylindrical shaped boundary). The strength of the perturbations associated with FCB increases with increasing flow speed so that at lower Alfven Mach numbers (~5–8) the boundary resembles a magnetosonic pulse. At higher speeds, it steepens to form a shock front associated with factors of 2–3 jumps in the background density and magnetic field. Normals to the FCB lie nearly perpendicular to the solar wind flow direction. The flow diversions associated with the pair of FCBs are in opposite directions away from the Sun-Earth line. In other words, FCBs participate in flow diversion around the obstacle and are in essence, an extension of the bow shock.

[26] To further understand the Mach number dependence of FCBs, we used local hybrid simulations to determine their properties as a function of ion beam density, velocity and temperature. The perturbations associated with the FCBs increase with increasing beam density or velocity but are far less sensitive to beam temperature. The formation and strength of the FCB is tied to the generation and nonlinear evolution of ULF waves excited along and at very large angles to the magnetic field in the foreshock region. The growth rates of these waves increase with increasing beam density and velocity leading to larger wave amplitudes and more enhanced FCBs. The effect of beam temperature on growth rates is less pronounced and therefore, FCB strength is less sensitive to this parameter (at least for the beam temperatures considered here). While FCB formation is a kinetic process, a simple fluid argument can describe its formation by noting that the presence of backstreaming ions results in increased pressure within the foreshock region leading to its expansion against the pristine solar wind and the generation of FCBs. The fact that FCB strength is not sensitive to beam temperature, however, demonstrates the limitation of a fluid picture in describing all of the FCBs properties.

[27] Our results indicate that FCBs form at cone angles of 10°, 20° and 40° and demonstrate that depending on the Mach number this boundary forms over a wide range of cone angles. While a pair of FCBs form at small cone angles, the results at $\theta = 20°$ and 40° show the formation of a single FCB. The cause of this asymmetry is tied to the

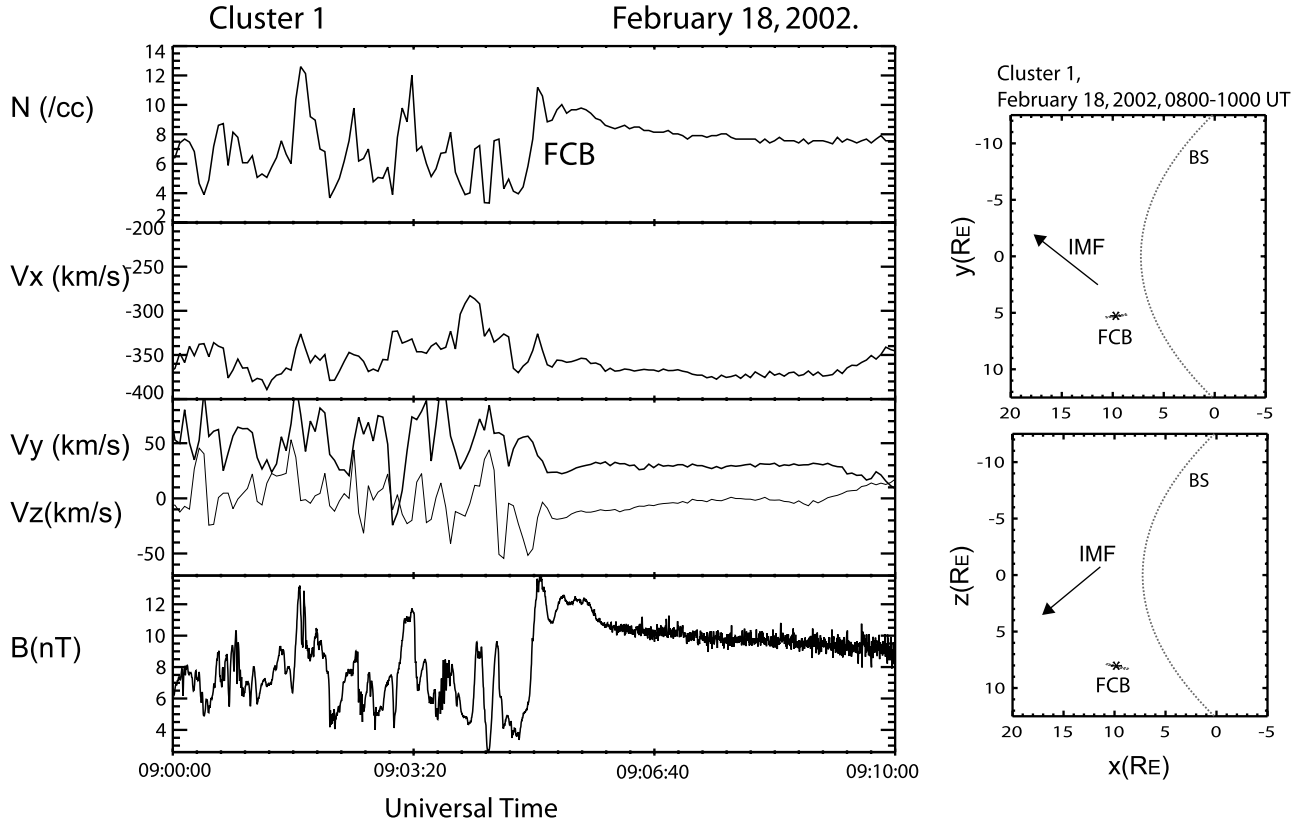

Figure 10. (left) Density, velocity components, and field magnitude illustrating the structure of a FCB observed by Cluster 1 on 18 February 2002, when $\theta_{VB} \approx 35°$. In this plot we use magnetic field data at a resolution of 5 vectors per second and spin resolution plasma moments from the CIS instrument provided by the CCA Cluster facility. A solid black (gray) line indicates the value of v_y (v_z). (right) The trajectory of Cluster 1 (solid line through the asterisk) in relation to a nominal bow shock from 0800 to 1000 UT on the xy and xz planes in GSE coordinates. The location of the FCB is marked with an asterisk.

variations of the beam properties originating from different parts of the parallel and quasi-parallel bow shock.

[28] In general, the FCB and ion beam and ULF foreshock boundaries do not coincide although at times the FCB separates the pristine solar wind from the ion foreshock plasma. As such, the FCB does not represent a boundary that marks the transition from quasi-parallel to quasi-perpendicular geometries at the bow shock. Instead, formation of the FCB is tied to the strength of ULF wave activity and the resulting drops in density and magnetic field strength in parts of the foreshock where this activity is strong. Because of the dynamic nature of the FCB and foreshock and the fact that ion beam properties originating from parallel and quasi-parallel portions of the bow shock have different properties (i.e., density or velocity) not all regions of the ion foreshock are associated with strong ULF activity and significant drops in density and magnetic field. As a result, the FCB can form well within the foreshock and away from the ion and ULF foreshock boundaries. Because, regions of the foreshock connected to parallel and nearly parallel bow shock are associated with stronger beams and ULF waves, the FCB typically forms in association with this activity and initially may separate the foreshock from the pristine solar wind. At later times however, ions originating from other parts of the bow shock reach this pristine solar wind and the FCB falls behind the ion foreshock boundary. As a rule we expect that in the earlier stages of their formation FCBs separate the pristine solar wind from the foreshock plasma. However, further in their evolution one may find backstreaming ions and ULF waves beyond the FCBs.

[29] Using an example of a FCB in the Cluster data we have shown that the characteristics of the simulated FCB are in good general agreement with the observations. More extensive studies are needed and being carried out to compare the predictions of the model with observations of the FCBs in more detail.

[30] **Acknowledgments.** Work for this project was supported by NASA grant NNX08AF38G to Solana Scientific Inc. and GSFC and by NSF grant ATM-0502992. We thank the Cluster FGM team, the Cluster CIS instrument team, and the ESA CAA Cluster facility for the data provided through their Web page.

[31] Zuyin Pu thanks Karlheinz Trattner for his assistance in evaluating this paper.

References

Asbridge, J. R., S. J. Bame, and I. B. Strong (1968), Outward flow of protons from the earth's bow shock, *J. Geophys. Res.*, *73*, 5777–5782, doi:10.1029/JA073i017p05777.

Balogh, A., et al. (2001), The Cluster Magnetic Field Investigation: Overview of in-flight performance and initial results, *Ann. Geophys.*, *19*, 1207–1217.

Blanco-Cano, X., N. Omidi, and C. T. Russell (2006), Macro-Structure of Collisionless Bow Shocks: 2. Wave properties, *J. Geophys. Res.*, *111*, A10205, doi:10.1029/2005JA011421.

Blanco-Cano, X., N. Omidi, and C. T. Russell (2009), Global hybrid simulations: Foreshock waves and cavitons under radial IMF geometry, *J. Geophys. Res.*, *114*, A01216, doi:10.1029/2008JA013406.

Bonifazi, C., A. Egidi, G. Moreno, and S. Orsini (1980a), Backstreaming ions outside the Earth's bow shock and their interaction with the solar wind, *J. Geophys. Res.*, *85*, 3461–3472, doi:10.1029/JA085iA07p03461.

Bonifazi, C., G. Moreno, A. J. Lazarus, and J. D. Sullivan (1980b), Deceleration of the solar wind in the Earth's foreshock region: ISEE 2 and IMP 8 observations, *J. Geophys. Res.*, *85*, 6031–6038, doi:10.1029/JA085iA11p06031.

Fuselier, S. A. (1995), Ion distributions in the Earth's foreshock upstream from the bow shock, in *Physics of Collisionless Shocks*, edited by C. T. Russell, *Adv. Space Res.*, *15*(8–9), 43–52.

Gary, S. P., J. T. Gosling, and D. Forslund (1981), The electromagnetic ion beam instability upstream of the Earth's bow shock, *J. Geophys. Res.*, *86*, 6691–6696, doi:10.1029/JA086iA08p06691.

Gosling, J. T., J. R. Asbridge, S. J. Bame, G. Paschmann, and N. Sckopke (1978), Observations of two distinct populations of bow shock ions in the upstream solar wind, *J. Geophys. Res.*, *5*, 957–960.

Greenstadt, E. W., et al. (1968), Strong, correlated magnetic field and plasma observations of the Earth's bow shock, *J. Geophys. Res.*, *73*, 51–60, doi:10.1029/JA073i001p00051.

Greenstadt, E. W., C. T. Russell, and M. Hoppe (1980), Magnetic field orientation and suprathermal ion streams in the Earth's foreshock, *J. Geophys. Res.*, *85*, 3473–3479, doi:10.1029/JA085iA07p03473.

Hoppe, M. M., C. T. Russell, L. A. Frank, T. E. Eastman, and E. W. Greenstadt (1981), Upstream hydromagnetic waves and their association with backstreaming ion populations: ISEE 1 and 2 observations, *J. Geophys. Res.*, *86*, 4471–4492, doi:10.1029/JA086iA06p04471.

Lapenta, G. (2002), Particle rezoning for multidimensional kinetic particle-in-cell simulations, *J. Comput. Phys.*, *181*, 317–337, doi:10.1006/jcph.2002.7126.

Narita, Y., et al. (2004), Alfvén waves in the foreshock propagating upstream in the plasma rest frame: Statistics from Cluster observations, *Ann. Geophys.*, *22*, 2315–2323.

Omidi, N. (2007), Formation of foreshock cavities, in *Turbulence and Nonlinear Processes in Astrophysical Plasmas*, edited by D. Shaikh and G. Zank, *AIP Conf. Proc.*, *932*, 181.

Omidi, N., and D. Sibeck (2007), Formation of hot flow anomalies and solitary shocks, *J. Geophys. Res.*, *112*, A01203, doi:10.1029/2006JA011663.

Omidi, N., et al. (2004), Dipolar magnetospheres and their characterization as a function of magnetic moment, *Adv. Space Res.*, *33*(11), 1996, doi:10.1016/j.asr.2003.08.041.

Omidi, N., X. Blanco-Cano, and C. T. Russell (2005), Macrostructure of collisionless bow shocks: 1. Scale lengths, *J. Geophys. Res.*, *110*, A12212, doi:10.1029/2005JA011169.

Paschmann, G., N. Sckopke, S. J. Bame, J. R. Asbridge, J. T. Gosling, C. T. Russell, and E. W. Greenstadt (1979), Association of low-frequency waves with suprathermal ions in the upstream solar wind, *Geophys. Res. Lett.*, *6*, 209–212, doi:10.1029/GL006i003p00209.

Reme, H., et al. (2001), First multispacecraft ion measurements in and near the Earth's magnetosphere with the identical Cluster Ion Spectrometry (CIS) experiment, *Ann. Geophys.*, *19*, 1303–1354.

Russell, C. T., and M. Hoppe (1983), Upstream waves and particles, *Space Sci. Rev.*, *34*, 155–172, doi:10.1007/BF00194624.

Sibeck, D. G., T.-D. Phan, R. Lin, R. P. Lepping, and A. Szabo (2002), Wind observations of foreshock cavities: A case study, *J. Geophys. Res.*, *107*(A10), 1271, doi:10.1029/2001JA007539.

Sibeck, D. G., N. Omidi, I. Dandouras, and E. Lucek (2008), On the edge of the foreshock: Model-data comparisons, *Ann. Geophys.*, *26*, 1539–1544.

Thomas, V. A., and S. H. Brecht (1988), Evolution of diamagnetic cavities in the solar wind, *J. Geophys. Res.*, *93*, 11,341–11,353, doi:10.1029/JA093iA10p11341.

Winske, D., and N. Omidi (1993), Hybrid codes: Methods and applications, in *Computer Space Plasma Physics: Simulation Techniques and Software*, edited by H. Matsumoto and Y. Omura, pp. 103–160, Terra Sci., Tokyo.

Winske, D., and N. Omidi (1996), A nonspecialist's guide to kinetic simulations of space plasmas, *J. Geophys. Res.*, *101*, 17,287–17,303, doi:10.1029/96JA00982.

X. Blanco-Cano, Ciencias Espaciales, Instituto de Geofisica, Universidad Nacional Autonoma de Mexico, Coyoacan, Mexico 04510.

N. Omidi, Solana Scientific Inc., Solana Beach, CA 92075, USA. (omidi@solanasci.com)

D. G. Sibeck, NASA Goddard Space Flight Center, 8800 Greenbelt Road, Greenbelt, MD 20771, USA.